28

Compact Electrostatic Coalescer Technology

Olav Urdahl
Veslefrikk Operations, Statoil, Sandsli, Norway

Nicholas I. Wayth
BP Amoco Exploration, Greenford, Scotland

Harald Førdedal
Statoil A/S, Trondheim, Norway

Trevor J. Williams and Adrian G. Bailey
University of Southampton, Southampton, Hampshire, England

I. INTRODUCTION

In the offshore production of petroleum, technical problems are sometimes encountered with emulsions which are formed at different stages of the production and transportation processes. These have to be taken into consideration at an early stage of the planning and construction of a platform. Enough space must be reserved for emulsion destabilization equipment such as coalescers and separators. With effective methods of emulsion separation, based on reliable information about crude oil and its tendency to form emulsions, much of this space could be reserved for other more useful purposes.

The stability of water-in-crude oil emulsions has been investigated thoroughly during the last 20 years, which has resulted in an increased understanding of the underlying mechanisms (1-17). This information could be utilized in order to develop more efficient chemical demulsifiers and, as a result, improve the separation efficiency of platforms. Another way of improving separation efficiency is to establish more refined or new methods of physical separation. In this chapter, the electrostatic destabilization of water-in-oil emulsions under flowing conditions is investigated.

II. HISTORICAL OVERVIEW

In the petroleum industry, the first work on electrocoa-lescence dates back to the beginning of the 20th century when Cottrell applied external electric fields to crude-oil emulsions (18, 19). Subsequently, much effort has been made to gain a deeper understanding of the processes taking place during the breaking of oil-continuous emulsions in electric fields (20-27). Allan and Mason (21) examined the application of a d.c. electric field to a water-heptane system containing surfactant. They concluded that the rate of film drainage was significantly enhanced by the electric field, resulting in a reduced droplet lifetime. This conclusion was later confirmed by Brown and Hanson (22, 23) for water-in-kerosene emulsions subjected to an a.c. electric field.

Bailes and Larkai (24) used insulated electrodes energized by the application of a pulsed d.c. field. The main advantage of this approach is that short-circuiting, due to water slugs or droplet chains bridging the electrodes, can be avoided. Galvin (25), who also employed insulated electrodes, emphasized the importance of using a properly designed power supply.

Taylor (26) investigated the influence of high-voltage

electric fields on the stability of water-in-crude oil emulsions. He concluded that two types of behavior (termed types I and II) occur, which are related to the rheological properties of the crude oil/water interface. For incompressible crude oil/water films, it was proposed that chains of water molecules formed which hindered droplet coalescence and increased the conductivity of the emulsion (type I behavior). However, efficient coalescence of water droplets was thought to be associated with a minimal increase in the electrical conductivity of the emulsion. It was suggested that this could be explained by the interfacial film being compressible (type II behavior). These findings were later verified by Chen et al. (27).

Gestblom et al. (28) used dielectric spectroscopy to investigate the behavior of concentrated water-in-oil emulsions stabilized by C9PhE4 and subjected to strong electric fields. They concluded that the breakdown process of emulsions built up gradually. The reason for this was believed to be an angular dependence of the membrane potential between closely packed droplets. This implies that droplet pairs aligned parallel to the applied electric field have the highest probability of coalescence. Further, the membrane potential was found to be directly dependent on droplet size. Thus, in a polydisperse emulsion, the electric field required to promote coalescence is inversely related to droplet size since, for a given applied field strength, the membrane potential increases with droplet size.

Conventional electrocoalescers are large vessels containing electrodes, between which a "treating space" exists where dispersed water droplets grow mainly by electrocoalescence, and a "settling zone" where phase separation takes place under laminar-flow conditions. A considerable residence time, typically 30-40 min, is required, hence the need for large vessels. This leads to problems offshore where, in order to economize on platform structure, an important issue is the reduction of weight and size of topside equipment. By decoupling the electrocoalescence and phase separation processes, it should be possible to obtain droplet growth in laminar or turbulent flow and subsequently separate the phases by using conventional equipment (centrifugal separation is also an option). This should make it feasible to reduce the size, weight, and residence time of separation equipment.

III. THEORETICAL OVERVIEW

An understanding of the droplet size distribution created during flow mixing of immiscible fluids has long been of importance to the chemical engineering industry. The nature of both the size distribution of dispersed droplets and the mean droplet size affect many chemical processes and are of great significance to the study of coalescence and phase separation. In this section, the mechanisms which cause droplet break-up are examined and their effects compared.

A. Droplet Break-up Processes

1. Droplet Break-up due to Turbulent-flow Conditions

Kolmogorov (29) is believed to have been one of the first workers to investigate droplet break-up in dispersed systems. For turbulent flow, Kolmogorov determined the microscale eddy length to be:

$$\eta = \left(\frac{\nu_c^3}{\varepsilon}\right)^{0.25} \tag{1}$$

where ϵ is the turbulent energy dissipation rate per unit mass, and ν_c is the kinematic viscosity of the continuous phase. Kolmogorov also determined a time microscale by combining the two parameters ϵ and ν_c in a different way:

$$\tau = \left(\frac{\nu_c}{\varepsilon}\right)^{1/2} \tag{2}$$

For droplets of diameter smaller than the Kolmogorov microscale (d < n) and with a relaxation time less than the time microscale ($T_r < T$, where $T_r = d^2/18\nu_c$), local viscous stress forces dominate. However, for droplets larger than the Kolmogorov microscale (d > n), dynamic pressure effects dominate droplet and inter-droplet processes. From calculations based on the experimental systems used in studies at Southampton University (which employed rectangular and annular ducts), estimates of the Kolmogorov microscale η were made. In the rectangular ducts, these range from around 300 μm, at the onset of turbulence, down to around 60 μm in the outlet pipe-work at high flow rate. The droplet diameters examined ranged from around 1 μm to over 1000 μm, indicating that, under different conditions, droplet diameters may be below or above the Kolmogorov microscale and therefore that both regimes are relevant.

Hinze (30) investigated the splitting of globules under different flow regimes and identified three different types of droplet deformation: "lenticular," "cigarshaped," and "bulgy." Lenticular deformation commences with a globule being flattened into an oblate ellipsoid. The subsequent stages leading to break-up depend on the magnitude and type of external forces causing the deformation. Hinze gave

the example of a droplet deforming into a torus before breaking into many droplets. The cigar-shaped deformation is defined by elongation of a droplet into a long cylindrical thread which subsequently becomes unstable and breaks up into smaller droplets. Bulgy deformation occurs when the surface of a droplet is deformed locally; protuberances appear and the droplet becomes irregular in shape.

Hinze also discussed various well-defined flow forms and the types of droplet deformation associated with them. The flow patterns described are: parallel flow, plane hyperbolic flow, rotating flow, axisymmetric hyperbolic flow, Couette flow, and irregular flow (turbulent).

In the case of droplet deformation and break-up in dynamic pressure flow, Hinze (30) estimated the maximum stable droplet diameter (d_{max}) under turbulent shear conditions to be:

$$C = d_{\max}\left[\frac{\rho_c}{\gamma}\right]^{0.6}\varepsilon^{0.4} \tag{3}$$

where p_c is the continuous phase density, and y is the interfacial tension between the two phases.

Hinze interpreted data from Clay (31) in order to determine a value of 0.725 for C which allows the diameter d_{95} in Couette flow to be deduced [see Eq. (4)]. Karabelas (32) questioned the assumptions made in Eq. (3), as turbulent flows are sometimes neither isotropic nor homogeneous. However, a number of workers have found the expression to be satisfactory. The d_{95} diameter may also be expressed as a function of the Weber number:

$$\frac{d_{95}}{D} = 1.516\left[\frac{\gamma}{D\rho_0 \bar{U}^2}\right]^{0.6}\mathrm{We}^{0.10} \tag{4}$$

where D = pipe diameter, and $Dp_c[dO]U[/dO]^2/y$ = We (Weber number).

Sleicher (33) carried out experimental work using a pipe section, of length 14.6 m and internal diameter 38 mm, in which droplets of uniform size were accelerated. The diameter d_{max} was arbitrarily defined as the initial drop diameter for which 20% of the droplets broke up. Taking into account viscous forces, Sleicher derived the following expression:

$$\left[\frac{d_{\max}\rho_c \bar{U}^2}{\gamma}\right]\left[\frac{\mu_c \bar{U}}{\gamma}\right]^{0.5} = 38\left[1 + 0.7\left(\frac{\mu_d \bar{U}}{\gamma}\right)^{0.7}\right] \tag{5}$$

This differs from Eq. (4) in that it does not account for the pipe diameter D. However, later work by Paul and Sleicher (34) indicated a small dependency on pipe diameter given by $d_{max} \propto D^{0.1}$. Collins (35) questioned whether the flow length was sufficient for the droplets to have reached a stable maximum size.

Following experimental and theoretical work on water-in-oil emulsions, Karabelas found the Hinze expression [Eq. (3)] more accurate than that of Sleicher [Eq. (5)]. Further, Karabelas developed the following empirical expression for d_{max}:

$$\frac{d_{95}}{D} = 4.0\,\mathrm{We}^{-0.6} \tag{6}$$

where again, We = $Dp_c[dO]U[/dO]^2/y$ (Weber number). Based on experimental results, Karabelas found Eq. (6) to be superior to both the Hinze and Sleicher expressions since it offers reliability throughout the range of practical Reynolds numbers (Re). However, caution was recommended for very viscous systems where inertial forces also influence droplet break-up.

2. Droplet Break-up Due to Laminar-flow Conditions

Droplet break-up under laminar-flow conditions is less prevalent than under turbulent flow owing to the lower energy dissipation in the fluid. However, shear stress may still cause the break-up of larger droplets, particularly if the fluid flow rate is at a fairly high level, approaching the turbulent regime. The fluid shear, for a given geometry, is greatest at the boundaries and vanishes along the line of maximum flow velocity. Rumscheidt and Mason (36) suggested that droplets undergoing shear from a velocity gradient disintegrate when the dimensionless velocity gradient group (N defined below) reaches a critical value:

$$N = \tau_0 G \mu_c/\gamma \tag{7}$$

where r_0 is the maximum, stable, undistorted droplet radius (initial), and G is the shear rate.

The critical velocity gradient N_{crit} is dependent on the viscosities of the two phases and is defined as:

$$N_{crit} = \frac{1}{2}\left[\frac{1+k}{1+19k/16}\right] \tag{8}$$

where k is the ratio of dispersed-phase viscosity to continuous-phase viscosity μ_d/μ_c. N_{crit} varies between limits of 0.50 and 0.42 for the entire range of viscosity ratios. For a typical water-in-oil system, K is at the higher end of this scale.

3. Droplet Break-up Due to Electrostatic Forces

An electrostatic field applied across an emulsion will place a limit on the maximum stable droplet size. The electrostatic field has a polarizing effect which creates charges of opposite polarity at opposing sides of the droplet. This elongates the droplet, in the direction of the applied electric field, and may result in break-up if the disruptive electrostatic force exceeds the cohesive interfacial force.

Rosenkilde (37) described the shape of a droplet subjected to an electrostatic field as a prolate ellipsoid (rugby ball shaped). The relationship between electrostatic forces and interfacial forces acting on droplets is described by the electrostatic Weber number defined as follows:

$$\frac{d\varepsilon\, c\, E_0^2}{\gamma} = We_{crit} \tag{9}$$

The value of the critical Weber number We_{crit} was found by Rosenkilde to be 0.409 which compares well with the value of 0.41 derived by Wilson and Taylor (38). At the point of droplet break-up, Rosenkilde deduced also that the ratio of the semimajor to semiminor axes was 1.8391.

Williams (39) reviewed other electrostatic phenomena which hinder or counteract the coalescence of emulsion droplets under the action of an applied electrostatic field. These include: Taylor-cone formation, contact-separation charging, and droplet disruption due to the possession of charge. The formation of Taylor cones occurs when a conducting droplet is subjected to such a strong electric field that a conical protrusion is formed. This may subsequently lead to a jet which sprays many tiny droplets towards an oppositely charged or grounded object. These effects are well illustrated in work by Zeleny (40). Taylor (41) proved theoretically that the conical interface between two fluids can only exist at a semivertical angle of 49.29°. Experimentally, Taylor demonstrated that deviations beyond this angle result in instability.

A criterion for stability was shown to be:

$$\frac{V^2}{r_0}\gamma = C = 140 \tag{10}$$

where r_0 is the undistorted droplet radius, and V is the applied potential in electrostatic units (1 V = 1/300 esu and 1 Coulomb = 3×10^9 esu).

Using a surface tension of y = 37 mN m^{-1} and a relative permitivity of γ_r = 2.2, Taylor found the critical potential for transformer oil in his experimental apparatus to be:

$$\begin{aligned} V_{crit} &= 1.432 \times 10^3 \times (37)^{0.5} \times (1.25)^{0.5} \times (2.2)^{-0.5} \\ &= 6.5 \times 10^3\, V \end{aligned} \tag{11}$$

where 1.432×10^3 is a constant associated with the experimental geometry, and 1.25 is the height in centimeters of the upper disk electrode above the conical tip.

Experimentally, however, Taylor found the critical potential to vary slightly, two typical values being 7.2×10^3 V and 7.6×10^3 V. He explained the discrepancy in terms of molecular surface effects and imperfect insulation.

B. Droplet Coalescence Processes

The process of droplet coalescence may involve many different mechanisms. In simple terms, there are four stages in the coalescence of a droplet pair. First, the droplets must come into very close proximity, under long-range flocculation forces, before the second stage of film thinning occurs. The rate of thinning of the continuous-phase membrane, between two droplets, is dependent on droplet size, the level of deformation of the droplets, and the force between them. At the end of the film-thinning phase, the two droplets come into contact as the fourth and final stage of film rupture, and droplet coalescence occurs.

It is appropriate to consider first the influences of long-range flocculation or collision mechanisms. Depending on the size and movement of dispersed droplets, different mechanisms will play different roles in the collision process. In a compact electrostatic coalescer (CEC), Brownian motion, sedimentation, laminar shear, turbulent shear, or turbulent inertia may play a role in droplet movement owing to hydrodynamic effects. Additionally, electrophoretic and dielectrophoretic forces, arising from the applied electric field, may act on dispersed droplets.

1. Brownian Motion

The bombardment of suspended water droplets, by molecules in the surrounding oil phase, will impart forces on the droplets causing them to move (Brownian motion). Small droplets are more susceptible to this effect than larger ones and this may result in collisions between neighboring droplets. Friedlander and Wang (42) investigated the effect of Brownian motion on dispersions, and the droplet size distribution was found to be self-preserving. In a CEC, the dynamic forces created by laminar and

turbulent shear are likely to dominate the effects of Brownian movement.

2. Sedimentation

Sedimentation occurs when droplets are allowed to settle under the effect of gravity. According to Stokes' law, settling velocity is proportional to the droplet diameter squared. Larger droplets will therefore settle at greater velocities than the smaller ones, resulting in collisions between droplets of different sizes in a polydisperse system. This process is commonplace in large, conventional settling tanks. In a rapid through-flow unit, such as a CEC, sedimentary coalescence is more likely to occur at the lower flow rates, particularly for the larger water droplets. Sedimentary coalescence also occurs if a tangential inlet configuration is used in a CEC. Such an inlet design would accelerate the larger droplets to greater velocities than the smaller ones and result in collisions between the droplets. Any increase in the centripetal acceleration over gravity would produce a proportional increase in collision frequency. Even a relatively low centripetal acceleration, of say 100 m s^{-2} (many times lower than that produced by a centrifugal device such as hydrocyclone or centrifuge), would still give an order of magnitude increase in collision frequency.

3. Laminar Shear

Droplet collision under laminar shear can occur due to velocity differences between droplets in different streamlines. The collision rate is therefore proportional to the shear rate of the fluid and this implies that droplet collisions are more likely near the walls of a duct where the velocity gradient is greatest. The work of Allan and Mason (21) is of particular interest in this respect. They investigated the coalescence of droplets subjected to laminar shear with and without an imposed electric field. Silicone oil was used as the continuous phase and water (distilled water plus 0.07% KC1) for the dispersed phase. Two counter-rotating cylinders were used to create Couette flow of the oil, into which was placed a pair of charged or uncharged water droplets. The collision and coalescence mechanisms were observed, under a microscope, with and without an applied d.c. electric field. The coalescence of droplets without shear or an electric field, due to van der Waals' forces, was also observed (although these tests were aborted owing to erratic behavior probably caused by convection currents).

The injected droplets had diameters of 750 ± 25 μm. This represents the higher end of the droplet size distribution one would expect to find in a CEC, but the results are still of interest. The injected droplets were so large that deformation resulted, which led to asymmetrical paths of approach and recession. The path of recession was found to be at a smaller angle than that of the approach. This contrasts with the behavior of rigid droplets, investigated using 500-μm polystyrene spheres, where symmetry was observed in the approach and recession paths. With uncharged droplets, and an applied electrostatic field, the coalescence angle θ_c of the droplets, shown in Fig. 1, was found to decrease as the applied potential was increased. There was also a reduction in the coalescence time of droplets as the rate of film-thinning increased. However, at the highest field strength of 1000 V/cm, the droplets were seen to approach one another before suddenly moving apart. This was thought to be due to charge exchange, whereby the droplets were left with an equal and opposite charge, causing them to move apart in the applied electric field. When the applied field was removed, the droplets were once again attracted to one another, which resulted in coalescence.

With no applied electric field, Allan and Mason (21) made comparisons between doublet interactions with both droplets charged or one charged and the other uncharged. When both droplets were charged at the same level, repulsive effects were seen which increased as the potential was raised to + 250 V. Collision could be induced by increasing the shear rate from 0.15 to 4 s^{-1}. With one droplet charged, the paths of the droplets were the same as for uncharged droplets. However, at the highest applied potential, charge exchange was observed between the charged and uncharged droplets on contact. This left both droplets positively charged and caused repulsion between them. Coalescence could only then be induced by increasing the shear rate.

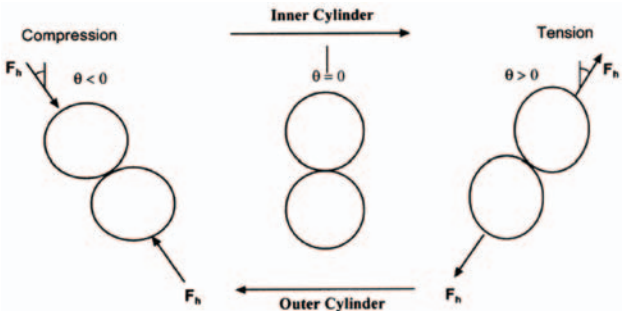

Figure 1 Collision of droplets under laminar shear.

4. Turbulent Collisions

Saffman and Turner (43) considered collisions between droplets due to turbulence in rain clouds. Under turbulent conditions, droplet collision is governed by two different mechanisms: isotropic turbulent shear and turbulent inertia. The choice of regime applicable to a droplet is determined by its size in relation to the Kolmogorov microscale η denned earlier. Droplets of diameter d > η are subjected to the former of these processes (small-scale motion). Spatial variations in the flow give neighboring droplets different velocities and this result in collisions. Droplets of diameter d > η are subjected to turbulent inertia. In this case, collisions result from the relative movement of droplets in the surrounding fluid. Droplets of different diameter will have different inertias and this results in collisions. Droplets of equal diameter, however, will not collide under this mechanism as they have the same inertia.

Saffman and Turner (43) produced collision expressions for droplet collisions governed by both small scale motion and turbulent inertia. The first of these is shown below:

$$N = 1.30\,(r_1 + r_2)^3\, n_1\, n_2 \left[\frac{\varepsilon}{\nu}\right]^{1/2} \qquad (12)$$

where ϵ and ν are as defined earlier and n_1 and n_2 are, respectively, the number densities of droplets having radii r_1 and r_2. This expression is valid for values of the ratio r_1/r_2 between 1 and 2. The multiplication factor 1.3 in Eq. (12) was later found to be incorrect by a factor of $\pi^{1/2}$ owing to an algebraic mistake. This was pointed out by Pearson et al. (44) who deduced a new factor of 2.3. In the case of turbulence inertia, the droplet collision rate is given by:

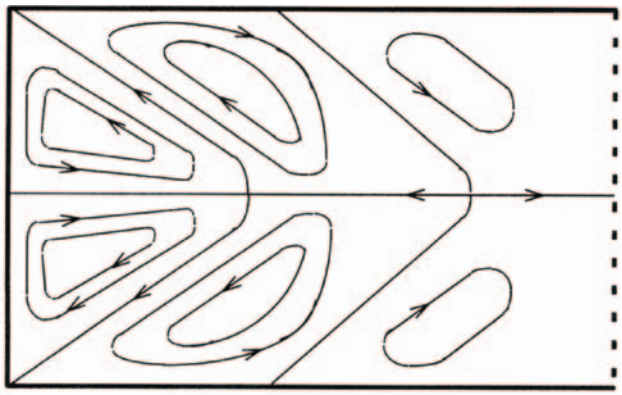

Figure 2 Secondary flow patterns in a rectangular duct based on Prandtl (45); cross sectional view of flow.

$$N = \frac{1.27(\rho_p - p_f)}{\mu}\left[\frac{\varepsilon^3}{\nu}\right]^{1/2} (r_1 + r_2)^2 \mid r_1^2 - r_2^2 \mid n_1 n_2 \qquad (13)$$

The efficiency of turbulence-induced collisions was found to be equivalent to that of gravity at a turbulent energy dissipation rate per unit mass of approximately ϵ = 2000 $cm^2\ s^{-3}$, which is equivalent to "vigorous turbulence." This shows that the turbulent growth of droplets in cumulus clouds might be sufficient to induce the formation of rain drops, but that in highlevel stratified clouds would be too low to initiate rainfall.

5. Secondary Flow Effects

The existence of secondary flow in a duct of rectangular cross-section was deduced by Prandtl (45) following measurements made by Nikuradse (46). There is a tendency for the liquid to flow toward the corners of the duct before returning to the center (as shown in Fig. 2). In the corners corners of the duct, where the shearing stress is less, flow moves from the inside to the duct wall. Where the shearing stress of the boundary is greatest, the flow is forced to the center of the duct due to turbulence.

The effects of secondary flow on droplet collision and coalescence mechanisms have not been considered in the literature currently reviewed. The scale of secondary flow is much larger than the Kolmogorov microscale η and it will, therefore, only affect droplets of diameter d > η (those subject to turbulent inertia). Secondary flow will be most prevalent following changes in duct geometry, particularly where there is some form of duct divergence.

6. Comparison Between Collision Mechanisms

Pearson et al. (44) compared the collision functions of various collision mechanisms, shown in Table 1. It is interesting to note that, although all the mechanisms shown are dependent on the continuous-phase properties, the droplet sizes, and the flow conditions, only sedimentation and turbulent inertia are dependent on the density difference between the dispersed and continuous phases. These two mechanisms only occur where the droplets are of different size, and their collision functions tend to zero as the droplet sizes become closer. From the collision functions of these two mechanisms it is seen that turbulent inertia will only dominate sedimentary coalescence when the characteristic acceleration is greater than that of gravity:

Table 1 Collision Functions and Dimensional Parameters for Various Processes

Mechanism	Collision function (β)	Source	Dimensional parameter
Brownian motion	$\frac{2kT}{3\mu}\frac{(r_i+r_j)^2}{r_i r_j} = 4\pi(D_i+D_j)(r_i+r_j)$	Smoluchowski (1916)	$K_B = \frac{kT}{\mu}$
Laminar shear	$1.33\,G(r_i+r_j)^3$	Smoluchowski (1917)	G
Pure strain (extension)	$4.89\dot{\gamma}(r_i+r_j)^3$	Zeichner and Schowalter (1977)	$\dot{\gamma}$
Isotropic turbulent shear	$2.3(r_i+r_j)^3\left(\frac{\varepsilon}{\nu}\right)^{0.5}$	Saffman and Turner (1956)	
Turbulent inertia	$1.27\frac{(\rho_p-\rho_f)}{\mu}\left(\frac{\varepsilon^3}{\nu}\right)^{0.25}(r_i+r_j)^2\lvert r_i^2+r_j^2\rvert$	Saffman and Turner (1956)	$\frac{\rho_p-\rho_f}{\mu}\left(\frac{\varepsilon^3}{\nu}\right)^{0.25}$
Differential sedimentation	$\frac{0.7g(\rho_p-\rho_f)}{\mu}(r_i+r_j)^2\lvert r_i^2+r_j^2\rvert$	Findeisen (1939)	$K_{ds} = \frac{g(\rho_p-\rho_f)}{\mu}$

$$1.27\left(\frac{\varepsilon^3}{\nu}\right)^{0.25} > 0.7g \tag{14}$$

The comparison between different collision mechanisms is examined further in the following section.

7. Collisions Due to Electrostatic Forces

Under an applied electric field, a droplet may be subject to two different electrostatic forces, depending on whether the drop is charged or neutral. Electrophoresis is the motion arising from the force exerted on a charged drop by the applied field:

$$F = \frac{q_1 q_2}{4\pi\varepsilon_0 r^2} \tag{15}$$

where q is the droplet charge. Clearly, the direction of motion is dependent on polarity of the charge and the applied field.

For a droplet charged by direct contact with an electrode, the predominant means by which a charging is likely to occur, the resultant force may be rewritten as:

$$F = \left[\frac{\pi^2}{6}\right]4\pi r^2\varepsilon_c E^2 \tag{16}$$

This force will cause a charged droplet to migrate toward an oppositely charged electrode. In doing so, it is likely to come into contact with other droplets, leading to coalescence. In a d.c. electric field, the droplet will migrate in a continuous path with its velocity determined by the viscosity of the continuous phase. The droplet will gradually lose its charge, depending on the relaxation time ϵ/σ of the continuous phase, and the driving force will diminish. In the case of an a.c. electric field, a charged droplet will tend to oscillate about its mean position between the electrodes.

A droplet may become charged by other mechanisms such as: ionization, preferential adsorption of ions at the interface (electric double layer), and droplet disintegration.

Neutral droplets can also be made to collide by inducing a dielectrophoretic force of interaction between neighboring droplets which arises from the polarization of the droplets in the applied electric field. The local electric field must be nonuniform, and the presence of the droplets will distort the field even if it is uniformly applied. The force, which is independent of field polarity, depends on the permittivity ϵ_c of the continuous phase and the volumes of the droplets. At larger separations, dielectrophoretic forces tend to be small in comparison with electrophoretic ones. However, at very close proximity, dielectrophoretic forces will dominate. The dielectrophoretic force acting on a droplet is given by:

$$F = 24\pi\epsilon_c E^2 r^2\left(\frac{r}{\delta}\right)^4 \text{ (large droplet separation)} \tag{17}$$

and at small separations ($\delta << r$) by:

$$F = \frac{2}{9}\pi^5 \varepsilon_c E^2 r^2 \frac{(r/h)}{\ln^2(r/h)} \quad \text{(small droplet separation)} \tag{18}$$

The different mechanisms described above have been compared graphically in Fig. 3. The factor $\epsilon_c E^2 r^2$ has been set to unity for all three mechanisms, and a relative force is plotted as a function of *r/h*.

The coalescence force *F* between two aligned droplets of equal size (radius *r*) in an applied electric field *E* was given, in electrostatic units, by Waterman (47) as:

$$F = 6\varepsilon_c E^2 \frac{r^6}{\delta^4} = 6\varepsilon_c E^2 r^2 \left[\frac{r}{\delta}\right]^4 \tag{19}$$

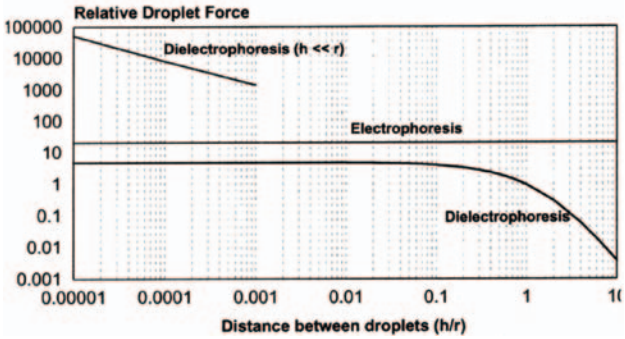

Figure 3 Comparison between droplet forces under electrophoresis and dielectrophoresis.

where ϵ_c is the dielectric constant of the continuous phase, and δ is the distance between droplet centers. Note that this differs from Eq. (17), which is presented in SI units, only by the factor $4_\pi\epsilon_0$, where ϵ_0 is the permittivity of free space. The difference only arises because of the different conventions used for the units. The r/δ part of Eq. (19) is proportional to the cube root of the water cut, and is therefore independent of average droplet size, unless sedimentation and phase separation occur.

The angle between two polarized equisized droplets, in relation to the applied electric field, plays a large role in the resultant force between them and therefore in their chance of collision. Work by Krasny-Ergen (48) gives zones of dipolar attraction and repulsion, as shown in Fig. 4. At large droplet separations, an attractive force exists for angles between $\theta = \pm 54.7^\circ$ from the direction of the applied electric field E_0. For droplets in contact, Krasny-Ergen gave the equivalent angle as $\theta = \pm 75.1^\circ$ (the limiting angle must vary as a function of the droplet separation). In both cases, the force between neighboring droplets is greatest when they are aligned with the electric field ($\theta = 0^\circ$). The presence of regions of repulsion is significant as it will hinder the collision and coalescence of droplets if they are outside the regions of attraction. However, a torque is established for droplets which initially repel one another. This rotates the droplets relative to one another so that the angle between them reduces, and attractive forces result. Fluid forces may also rotate droplet pairs into different angular orientations.

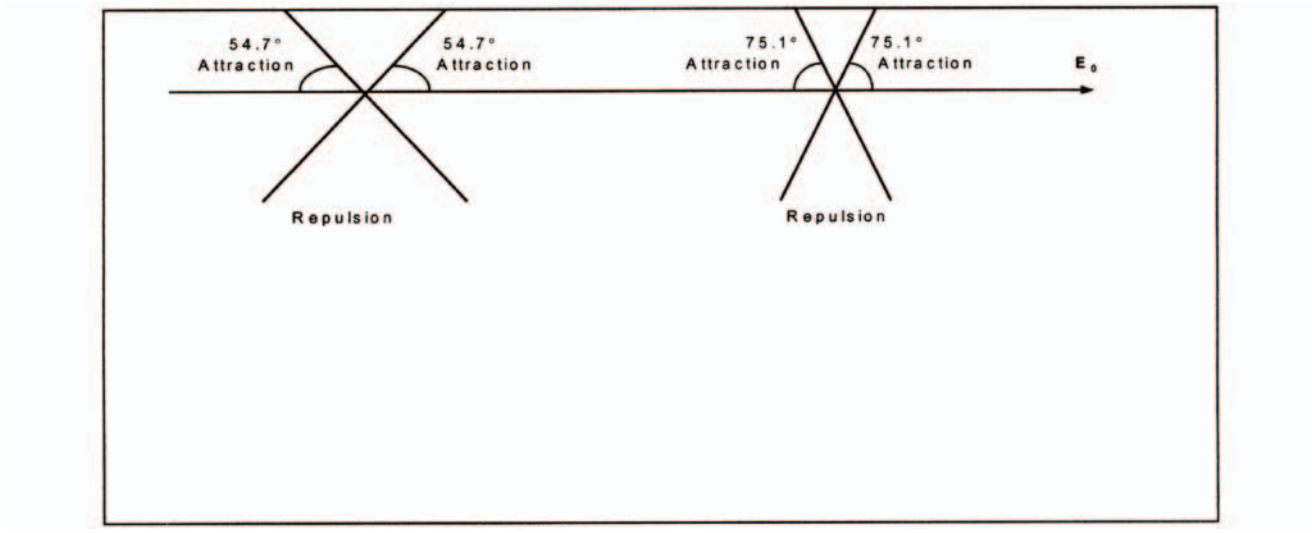

Figure 4 (left) Angles of attraction, two polarized droplets of large separation; (right) angles of attraction, two polarized droplets in contact.

8. Film Thinning and Droplet Coalescence

Once long-range flocculation of droplets has taken place, due to whatever hydrodynamic and electrostatic forces are present, film thinning occurs between adjacent droplets. The chances of coalescence will depend on the rate of film thinning and the forces holding the droplets together. The film-thinning rates depend on whether or not droplet deformation occurs and were considered by Williams (39):

$$\frac{dh}{dt} = \frac{-8\pi\gamma^2 h^3}{3\mu_c r^2 F} \quad \text{(deformable droplets)} \quad (20)$$

$$\frac{dh}{dt} = \frac{-2Fh}{3\pi\mu_c r^2} \quad \text{(nondeformable droplets)} \quad (21)$$

Equations (20) and (21) may be considered in terms of the electric field strength applied across a dispersion:

$$\frac{dh}{dt} = \frac{-12\gamma^2 h^4 \ln^2(r/h)}{\pi^4 \mu_c r^5 \varepsilon_c E_0^2} \quad \text{(deformable droplets)} \quad (22)$$

$$\frac{dh}{dt} = \frac{-4\pi^4 r \varepsilon_c E_0^2}{27\mu_c \ln^2(r/h)} \quad \text{(nondeformable droplets)} \quad (23)$$

Williams plotted the film-thinning time for deformable and nondeformable droplets against droplet radius. While an increase in droplet size increases the time required for thinning of a deformable droplet, nondeformable droplets experience a reduction in film thinning time as their size increases. It is interesting also to note the square relationship on thinning rate with nondeformable droplets and an inverse square relationship for deformable droplets. Clearly, increasing the applied field across a system with deformable droplets could result in a reduction in coalescence efficiency.

Oweberg et al. (49) looked at droplet coalescence mechanisms. By pressing together two droplets suspended on platinum wires (using a rack and pinion arrangement) and applying an electrical potential, the mechanisms of coalescence were studied using a highspeed camera. As water drops were held together the interface between them was seen to flatten and a "lens" appeared. This eventually disappeared and the two droplets coalesced. Oweberg described coalescence as the formation of intermolecular bonds across the interface between the drops. Two mechanisms were then described, by which bonds could be switched from within the droplets to across the interface. In the first mechanism, bonds were assumed to be broken then reformed in a process equivalent to evaporation followed by condensation. This mechanism occurred above a threshold potential difference (typically 6 V), and the rate of coalescence was found to be proportional to $\epsilon_d V^2$ (where ϵ_d is the relative permittivity of the water forming the droplets). In the case of the second mechanism, at potential differences below the threshold level, bonds were assumed to be gradually rearranged rather than broken in a process equivalent to diffusion. The rate of coalescence in this instance is given by $(\epsilon_d - 1)^{1/2}$ V. From Oweberg's work it is clear that the rate of coalescence is increased as the potential difference between two adjacent droplets is increased. Kitchener and Musselwhite (50), following work by Mason et al. (21, 36), examined the approach of two dispersed droplets. Three situations were discussed, the first for large drops where the inertial forces outweigh the surface forces. Here, concave dimpling occurs (Fig. 5a) and liquid is trapped between the deflections. Coalescence will occur on the ring of the dimple, which is the thinnest area. If the droplets are smaller, they are depressed by contact but remain convex (Fig. 5b). Coalescence takes place on the center line of the two droplets, the closest point of contact, as film drainage occurs. Slowly moving larger droplets also coalesce in this way. In the third situation (Fig. 5c) a thin liquid lamella forms between the droplets. This tends to occur in the presence of surfactants.

C. Electrostatic Separation of Water-in-Oil Emulsions

A multitude of different methods have been used to separate oil from water and water from oil. These techniques include gravity differential (settling and centri fugal), as well as fil-

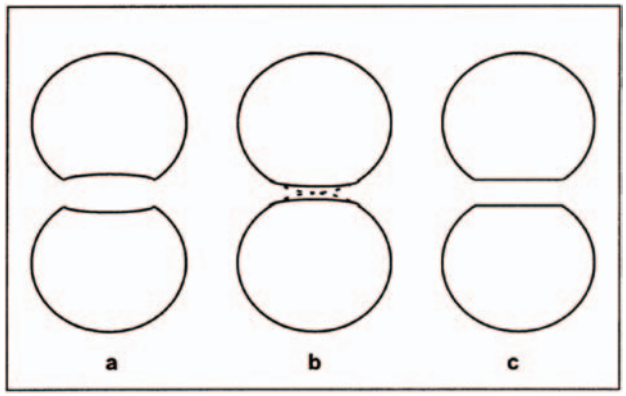

Figure 5 Basic mechanisms of droplet coalescence.

tration, membrane, ultrasonic, thermal, adsorption, electromagnetic, viscosity actuated, and Coanda techniques. Despite the myriad techniques available, both novel and conventional, the main technique employed to separate water from oil continues to be gravity separation using settling tanks, often enhanced by an electrostatic field, increased temperature, or destabilizing chemicals.

1. Conventional Electrostatic Dehydrators

As already reviewed, there are many papers on certain aspects of coalescence, but the literature available specifically on electrostatic coalescers is mainly in the form of patents. One of the most comprehensive papers is by Waterman (47), which discusses both commercial and scientific aspects (a rarity). Waterman explains the role of electrostatic coalescers in removing salts such as those of sodium, iron, and arsenic. Two coalescence mechanisms are explained: first, induced-dipole coalescence, which occurs in both a.c. and d.c. electric fields, and second, the coalescence resulting from the force produced by a unidirectional (d.c.) electric field acting on a charged droplet. The latter process is ineffective in an a.c. field. Dipole coalescence has been shown to be the dominant force, as coalescence occurs at least as efficiently in an a.c. electric field. Waterman developed one of the first models for electrocoalescence.

Sadek and Hendricks (51) were also responsible for developing a model for the electrical forces on suspended droplets. Taylor (26), again within an oil-industry context, carried out tests in which an electric field was applied to water-in-crude oil samples under a microscope. Three crude oils were used: Ninian, Kuwait, and Romashkino. Tests were carried out with 5% water at an applied voltage of 1 kV and with two additives. Two types of coalescence behavior were observed as discussed earlier. Type I behavior was defined as being related to droplet-chain formation. This caused an increase in emulsion conductivity and occurred in oils with incompressible interfacial films. Type II behavior was observed with low emulsion conductivities in high-strength electric fields, where droplets coalesced too quickly to form droplet chains. Taylor's joint work with Mohammed et al. (52—54) and Chen et al. (27) looked at many of the fundamental surface-chemistry topics relating to the dewatering of crude oil. Taylor (55) provides a comprehensive review of work in this area from both an industrial and academic viewpoint.

Mori et al. (56) carried out tests to break W/O emulsions in a small sample cell. Kerosene and 50 mol/m^3 hydrochloric acid were emulsified by using Rheodol SP-O10 surfactant (equivalent to Id's Span 80). Tests were carried out at frequencies between 40 and 2000 Hz at potentials of up to 8 kV. Coalescence was found to be enhanced with increase in frequency. Taking into account power requirements, 1000 Hz was found to be the most effective operating frequency. Phase separation was found to be faster for a smaller initial hold up of water but, with an aqueous content of less than 40%, coagulation occurred before coalescence and this slowed the process.

Wang et al. (57) investigated the demulsification of W/O emulsion by using an intense a.c. electric field. Their laboratory test cell consisted of an acrylic tube (7 cm in diameter and 10 cm high) with a metal plate attached to the base which acted as a grounded electrode. The energized electrode, which was insulated, was rather elaborate. It was formed by suspending an insulating beaker in the cell 2 to 6 cm above the grounded electrode. A copper wire was passed into the beaker to make contact with conductive aqueous sodium chloride solution contained inside. Silicone oil was floated on top of the liquid electrode to insulate the operator from electric shock. An emulsion was formed by suspending a mixture of an electrolyte (sulfuric acid) and deionized water (which formed the aqueous phase) in an organic phase of paraffin. Span 80 and ECA4360, both commercially available surfactants, were used to stabilize the emulsion. A mechanical homogenizer was used to shear the dispersed aqueous phase and vary the droplet size. Although not clearly stated, it would appear that all the tests were carried out at an aqueous phase concentration of 50% by volume. Measurements were made of the resolution time for the emulsion under varying conditions of electric field strength, initial droplet size, electrolyte concentration, and surfactant type and concentration.

The demulsification rate (k_w) was found to increase as a function of electric field strength as follows:

$$k_w \propto E^{0.626} \tag{24}$$

Similarly, k_w was found to increase as the initial droplet size was increased from a mean of 14.4 to 27.0 μm:

$$k_w \propto d^{2.21} \tag{25}$$

The exponent 2.21 determined by Wang et al. (57) was slightly lower than found by other workers; Hano et al. (58) and Fujinawa et al. (59) deduced k_w α $d^{3.5}$ and k_w, α d^3, respectively.

The increase in aqueous-phase electrolyte level was found to reduce k_w, despite increasing the density of the water and therefore the density difference between the two phases. Wang et al. claim that the reduction in k_w, at higher electrolyte concentrations, is due to an electric shielding effect which results in a reduction of the electrostatic force. However, the increase in electrolyte level will clearly affect both the physical and electrostatic properties of the aqueous phase, and this may explain the reduction in performance. A number of physical changes are likely. First, the overall conductivity of the emulsion increases, causing a reduction in the effective electric field strength across the emulsion. The nature of the electrical double layer may also change, perhaps increasing the repulsion between neighboring droplets. Additionally, the interracial tension between the two phases will be affected and this may further enhance emulsion stability.

2. Pulsed d.c. Waveform Systems

Bailes and Larkai (24) first experimented with the use of a pulsed d.c. waveform applied to a (W/O) emulsion. Early trials by these workers discovered problems with the use of d.c. and bare electrodes (in contact with the emulsion). Conducting droplets eventually created a short circuit from one electrode to the other or from an energized electrode to a nearby ground. These obstacles were overcome by the use of insulated electrodes and pulsed d.c. energization. Tests were carried out with acrylic insulation thickness of 3, 6, 10, and 13mm. Coalescence was found to be optimized when the d.c. applied voltage was modulated at low frequency. With a steady d.c. field, interfacial polarization occurs. This is a process whereby the insulation is charged to the opposite polarity of the adjacent electrode, and the electric field across the actual emulsion is greatly reduced, effectively ending electrostatically enhanced coalescence processes. Bailes and Larkai carried out experiments with two W/O systems. System A was based on Escaid 100, a kerosene-type hydrocarbon, with cyclohexane as the organic phase and water as the aqueous phase. System B was based on Escaid 100 with LIX 64N as the organic phase, and sulfuric acid in water as the aqueous phase. Tests were carried out with square, triangular, and semisinusoidal waveforms. Performance of the electrocoalescer was assessed in terms of the dispersion band depth in a subsequent gravity settling tank (a small dispersion band depth corresponds to efficient coalescence and vice versa).

This was extended by further work (60), which led to the formation of theoretical and experimental optimum frequencies for the pulsed d.c. system. An experimental optimum frequency for the system was found to lie between 8 and 10 Hz. At higher frequencies it was suggested that coalescence-enhancing droplet chains cannot form while, at lower frequencies, the droplet chains produce a current leakage path. A model was developed using a term for average droplet spacing and a function for the work done per collision, the force being produced by the applied electric field. The average number of collisions N was given as:

$$N = \frac{d \cdot I_m}{2.89\varepsilon\varepsilon_0 \cdot v_c \cdot E_{\max}\phi[(0.74/x)^{1/3} - 1]} \quad (26)$$

where d = distance between electrodes, l_m = mean conduction current, E_{max} = peak electric field strength, and Φ = fractional water hold-up.

For the system used by Bailes and Larkai (60), with Φ = 0.5 and an electrode area of A in contact with the emulsion, this becomes:

$$N = \frac{5}{\varepsilon\varepsilon_0 A} \bullet \frac{I_m}{E_{\max}} \quad (27)$$

The Bailes and Larkai model incorporates a number of assumptions such as the use of a monodispersion and uniform interdroplet spacing. However, developing a model incorporating a typical droplet distribution with random droplet spacing would be significantly more complicated. No attempt is made, either, to incorporate the effects of flow velocity or regime, and the experimental results do not indicate whether tests were carried out in laminar or turbulent flow (though laminar flow can be deduced). These parameters would also have had an effect on droplet collision frequency, and therefore the rate of coalescence.

Bailes and Larkai (61) investigated the effects of dispersed-phase hold-up. The optimum applied pulsed d.c. frequency was found not to be affected by the level of dispersed water hold-up. However, a minimum threshold level for water content (25%) was found, above which the best coalescence performance was produced. This was explained in terms of the drop size, which increases with rise in water cut, and the effective electric field, which reduces with rise in water cut. The optimum frequency for efficient coalescence was in the range 4-5.5 Hz. This is lower than the earlier value (8 Hz) as an acrylic insulation thickness of 3 mm rather than 6 mm was used.

Joos and Snaddon (62) did not agree with the ideas put forward by Bailes and Larkai (24, 60) to explain their experimental results. They argued that coalescence perform-

ance was an average field-strength effect and was not dependent on field frequency. The high-voltage pulsed d.c. power supply, used by Bailes and Larkai, incorporated a 100-Ω current-limiting resistor which connected the stabilized d.c. supply to the switching circuit. As the operational frequency was increased, the effective electric field applied to the emulsion reduced with consequent reduction in coalescence performance. If a smaller current-limiting resistance value had been chosen, the "optimum frequency" would have been increased. At frequencies below the "optimum frequency," interfacial polarization reduced the effective field strength across the emulsion by causing charge to build up at the emulsion/insulation interface (interfacial polarization). Joos and Snaddon produced a model based on Bailes and Larkai's work and argued that coalescence is a function of the mean value of the square of the effective electric field. Using a model based on Bailes and Lankai's work, they found an optimum frequency of 22 Hz, somewhat higher than the empirically derived 8 Hz. This is illustrated in Fig. 6 which shows an effective electric field applied to the emulsion as a function of operational frequency. It can be seen that at low frequencies the effective field strength is small owing to interfacial polarization. As the frequency is increased the effective field strength rapidly increases, reaching a maximum before it decreases due to the current-limiting resistor. Joos and Snaddon pointed out that their optimum frequency would be reduced from 22 to 8 Hz if the effective emulsion capacitance or resistance were to be increased by a factor of about 5.

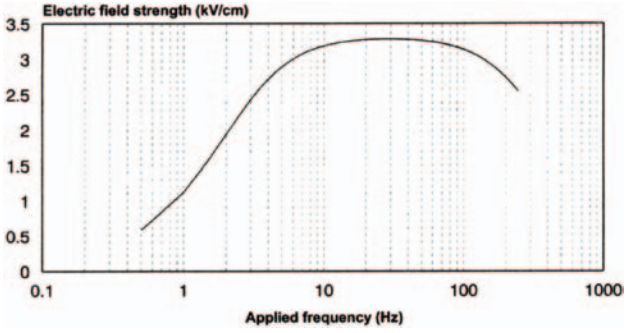

Figure 6 Frequency effects on effective electric field strength. The declining influence of interfacial polarization and the increasing influence of the current limiting resistor (10 MΩ) with frequency on effective field strength. Based on Φ = 0.15.

Bailes (64) has developed a mathematical model to explain previous experimental findings (24, 60). Taylor (55) provided further explanations of why there should be an optimum frequency. Gomis (65) investigated the work of Bailes and also of Joos and Snaddon. He pointed out that the model produced by Joos and Snaddon did not predict other trends found. For example, it did not explain why the optimum frequency is less critical at higher voltages, and why the optimum frequency is less for a thinner layer of insulation. Gomis extended Joos and Snaddon's model to include these parameters. The Gomis model is dynamic and therefore takes account of the applied electric field at all times. This is opposed to the Joos and Snaddon model which uses a time-averaged mean electric field value.

Drelich et al. (66) also performed tests on a laboratory rig to investigate the optimum frequency of a pulsed d.c. electric field on W/O emulsion separation efficiency. A mixture of 0.08-0.2 wt% distilled water and an aromatic extraction solvent were emulsified. The resulting emulsion was allowed to settle for 40 min to remove any large droplets. The viscous nature of the organic phase ensured that complete separation did not occur in this time. The emulsion was then pumped through an electrostatic cell of dimensions 150 mm (length) × 100 mm (width) × 70 mm (height). A bare cathode was fitted to the base of the cell and an insulated anode was fitted at the top of the cell. Epoxy resin was used to provide insulation thicknesses of 0.2 and 2.0 mm. A high-voltage pulse generator was used to apply an electric field across the emulsion at potentials of up to 20 kV and at frequencies between 5 and 25 Hz. The emulsion was then passed through a settler, and the separation efficiency was determined from the expression:

$$\text{Separation efficiency} = \frac{\phi_{inlet} - \phi_{outlet}}{\phi_{inlet}} \qquad (28)$$

A sharp increase in separation efficiency, from about 20 to 60%, was reported when the electrostatic field strength was increased from 0.32 to 1.33 kV/cm. When the field strength was increased further, up to a value of 10.6 kV/cm, only a small increase in separation efficiency was seen. This implied the presence of an optimum field strength. Additional measured values between electric field strengths of 0.32 and 1.33 kV/ cm would have been useful since the critical value may have been significantly lower than 1.33 kV/cm. Bailes and Larkai (61) reported critical field strengths of 0.3 kV/cm for concentrated emulsions and about 1 kV/cm for emulsions with a water hold-up of Φ < 0.09. Drelich et

al. (66) suggested that separation performance was optimized with pulsation frequencies of between 8 and 11 Hz, though not by more than 5-7%. They concluded that this improvement is of little practical significance. The paper fails to give details of the power supply and electric circuit used. Thus, it is not clear whether factors other than coalescence processes may have been influenced by the variations in frequency.

The question arises, therefore, whether an optimum frequency exists beyond that defined by the power-supply circuitry at high frequencies and the effects of interfacial polarisation at low frequencies.

IV. TECHNOLOGY STATUS

The only compact electrostatic coalescer that is commercially available at present is the Electro-Pulsed Inductive Coalescence (EPIC) (made by the National Tank Company (NATCO)). The EPIC device has a number of patents filed at this time; Ref. 67 shows a single-annulus down-flow unit. The W/O emulsion is injected tangentially at the inlet and swirls between the inside of the outer tubular vessel and an insulated inner electrode tube. An electric field is applied across the emulsion and that provided by a pulsed d.c. voltage is said to be preferable. It is claimed that this unit can improve water separation rates by as much as 1250% over conventional methods. Patents (68, 69) again relate to the EPIC device described in Ref.67 and, in addition, a double-annulus unit is described. As before, this incorporates a tangential inlet which causes the emulsion to swirl in the applied electric field. The emulsion first moves in down-flow, in the outer annular region, before its axial direction is reversed and it passes up into the inner annular region. The outer and inner annular regions are separated by an additional concentric electrode which allows an electric field to be applied to the emulsion before it passes upward out of the unit from the inner annular region. To facilitate the removal of any free water, which would be more likely in the outer down-flow region, an outlet is fitted at the bottom of the vessel. The use of a pulsed d.c. field, and an optimum frequency, is again mentioned in these patents but the use of other types of electrostatic field is not excluded.

During the first half of year 2000, Kvaerner Process Systems had planned to market a CEC. The theoretical framework for this design, for which a patent application was filed in 1998 (70), is based on work by Urdahl and coworkers (71, 72), Harpur et al. (73), and Wayth et al. (74).

This system, which has no inherent limitations with regard to water cut, is based on the use of a regular a.c. field (50-60 Hz) and insulated electrodes. The system has been shown to have a dramatic effect on the droplet growth in laboratory experiments (71, 73, 74) and in prototype testing it significantly improved the water/ oil separation rate of a downstream gravity settler (72).

Another type of CEC has been patented by Provost and Rojey (75, 76) but does not appear to be available commercially. This system is based on a combined centrifugal/electrocoalescer device for separating water from the oil. These two patents show a wide variety of compact configurations in which W/O emulsions are subjected to centripetal accelerations of up to 500 g in combination with applied electrostatic fields of strength up to 6 kV/cm. It is stated that the applied frequency of the a.c. electric field should preferably be between 50 and 60 Hz. The level of development of these devices in unknown but an efficient commercial version would certainly be of great interest to operators. The benefit of this type of approach is that larger droplets are separated immediately and there is less of a problem with droplet break-up in downstream pipework. However, such a CEC is necessarily larger and more complicated as it must incorporate a quiescent settling zone and apparatus for removing excess of water. Additionally, since this type of CEC contains a water/oil interface, it will be more susceptible to platform orientation and motion.

V. APPLICATIONS OF COMPACT COALESCERS

As more satellite fields are developed and connected to distant existing installations, efficient pipeline transport of multiphase, unprocessed well fluids is of increasing importance. The well fluid can contain large amounts of water which becomes emulsified in turbulent flow over several kilometers. As the well flow reaches the processing facilities, the system is choked, leading to further emulsification of the fluid system.

High water cuts often lead to a bottle-neck in the production process whereby the rate of oil production is constrained by large, undesired volumes of water. The problem is further compounded for emulsions which require longer residence times for separation. The stability of the emulsion formed depends on the properties of the oil. Heavy oils and oils which are acidic are more prone to forming stable emulsions. The viscosity of a W/O emulsion tends to be far higher than that of the oil itself, which, as a consequence,

increases pressure drop and reduces transport capacity.

The separation of water from oil is a major challenge in the processing of hydrocarbon fluids. There is a continual demand to improve the quality of crude oil before it is exported in pipelines or tankers to refineries. Stringent criteria restrict the maximum water content allowed in the export oil (normally 0.5% maximum) and the oil content of the effluent water (normally 40 ppm maximum). The separation of water from oil depends on several fluid- and system-dependent factors. Water not only leads to a threat of corrosion scale and hydrates, but can also dramatically increase pumping costs. First, the pumps must deal with a larger volume of fluid, and, second, the formation of a W/O emulsion can significantly increase fluid viscosity and thereby pressure drop in the pipeline (as mentioned above).

As demonstrated in other parts of this chapter, some advantages of the compact coalescer unit are: short residence times (seconds rather than many minutes), order-of-magnitude droplet growth, and effectiveness over a large range of water cut (1-30%).

A. Debottle-necking

The mixing of water and oil during production can cause very stable water-in-crude-oil emulsions. In addition to the mixing of water and oil in turbulent, multiphase flow, the fluid system is further mixed as the well stream is choked topside, ahead of the first-stage separator. In particular, heavy oils form stable W/O emulsions and, since the density difference is less, they are more difficult to separate. The location of a coalescer unit, upstream of the first-stage separator, increases the mean droplet size of the dispersed water. The consequences of this are: more effective phase separation, reduced residence time, a direct saving in chemical costs, and savings in heating costs if the process temperature can be reduced. Assuming that the level of demulsifier dosage can be reduced by 40 to 50%, it should be possible to save several million dollars in large oilfields.

B. Between Separator Stages

Large separators are needed to process water-in-crude-oil systems which require long residence times in the separation process. A series of three separators is often used for the purpose. Additional equipment, such as heaters and coalescers, as well as process plant for the treatment of produced water, may be connected to the separation train. This is especially true when processing heavy crude oils since it is possible for several per cent water to be left in the oil after the first stage of separation. Techniques for removing the remaining water may involve heating the oil between the first and second stages of separation. Alternatively, demulsifier or combinations of demulsifying chemicals may be added.

C. Alternative to Traditional Coalescer for Removing Remaining Water After Final Separation Stage

A traditional coalescer is the same size as a separator and hence is a large and heavy unit. If such a unit were to be replaced by a compact coalescer, a direct investment saving would result. Additionally, as the unit is smaller and lighter, a weight reduction in the production platform or ship on which it is mounted is possible.

D. Desalter at Refineries

So far, only the potential use of the compact coalescer in upstream processes has been considered. However, there is also potential for using the unit at refineries. In order to remove salt from a crude oil, fresh water is added to the oil and intimately mixed with it. In some cases, this water may stay in the oil for a long time. In order to remove this water, the oil must again be heated or treated with chemicals or both. The installation of a compact coalescer here can, therefore, provide a more effective desalting process.

VI. SUMMARY

This chapter has covered different physical phenomena and processes, ranging from bulk-fluid dynamics to microscopic interdroplet surface chemistry. All of these topics play a role in the electrostatic separation of W/O emulsions and the development and construction of an optimal, compact electrostatic coalescer. In some areas, such as turbulent droplet break-up, the understanding is well developed. In other fields there are still many questions to be answered. It is interesting to note that various authors have performed experimental assessments of W/O emulsion separation by using electrostatic fields. There is agreement on some as-

pects such as the general improvement in coalescer performance as the electric field strength is increased, to which the law of diminishing returns applies. In other areas, such as the existence of an optimum frequency for the applied electric field, there is still disagreement between researchers.

It is apparent that there are many different mechanisms working simultaneously when a W/O emulsion is treated in an electrostatic coalescing device. The overall growth of droplets is a balance of numerous hydrodynamic, electrostatic, chemical, and physical properties of the emulsion being treated. Some of these factors are double-edged swords, with both beneficial and detrimental effects on droplet growth. While high levels of turbulence or electric field strength promote the collision and coalescence of the smaller droplets, both mechanisms increase the chances of larger droplet break-up. Optimal droplet growth is therefore a careful balancing act of all of the factors, which must be carefully incorporated into the design of CECs.

ACKNOWLEDGMENT

Statoil is acknowledged for giving permission to publish the results.

REFERENCES

1. TJ Jones, EL Neustadter, KP Whittingham. J Can Petrol Technol 17: 100, 1978.
2. DG Thompson, AS Taylor, DE Graham. Colloids Surfaces 15: 103, 1985.
3. VB Menon, DT Wasan. Colloids Surfaces 19: 89, 1986.
4. VB Menon, DT Wasan. Colloids Surfaces 19: 107, 1986.
5. VB Menon, DT Wasan. Cooloids Surfaces 23: 353, 1987.
6. VB Menon, AD Nikolov, DT Wasan. J Colloid Int Sci 124: 317, 1988.
7. VB Menon, DT Wasan. Colloids Surfaces 29: 7, 1988.
8. EJ Johansen, IM Skjørvø, T Lund, J Sjøblom, H Søderlund, G Bostrøm. Colloids Surfaces 34: 353, 1988/89.
9. J Sjøblom, H Søderlund, S Lindblad, EJ Johansen, IM Skjærvø. Colloid Polym Sci 268: 389, 1990.
10. J Sjøblom, L Mingyuan, H Høiland, EJ Johansen. Colloids Surfaces 46: 127, 1990.
11. J Sjøblom, O Urdahl, H Høiland, AA Christy, EJ Johansen. Progr Colloid Polym Sci 82: 131, 1990.
12. KG Nordli, J Sjøblom, J Kizling, P Stenius. Colloids Surfaces 57: 83, 1991.
13. J Sjøblom. ed. Emulsions —- A Fundamental and Practical Approach. NATO ASI Series. Dordrecht: Kluwer Academic, 1992.
14. L Mingyuan. PhD thesis, University of Bergen, Norway, 1993.
15. O Urdahl. PhD thesis, University of Bergen, Norway, 1993.
16. O Urdahl, AE Møvik, J Sjøblom. Colloids Surfaces A 74: 293, 1993.
17. B Balinov, O Urdahl, O Søderman, J Sjøblom. Colloids Surfaces A 82: 173, 1994.
18. FG Cottrell. US Patent 987 114, 1911.
19. FG Cottrell, JB Speed. US Patent 987 115, 1911.
20. TJ Williams, AG Bailey. IEEE Trans Ind Appl IA-22: 536, 1986.
21. RS Allan, SL Mason. Trans Faraday Soc 57: 2027, 1961.
22. AH Brown, C Hanson. Trans Faraday Soc 61: 1754, 1965.
23. AH Brown, C Hanson. Chem Eng Sci 23: 841, 1968.
24. PJ Bailes, SKL Larkai. Trans Inst Chem Eng 59: 115, 1981.
25. CP Galvin. Inst Chem Eng Symp Ser (No. 88): 101, 1984.
26. SE Taylor. Colloids Surfaces 29: 29, 1988.
27. TY Chen, RA Mohammed, AI Bailey, PF Luckham, SE Taylor. Colloids Surfaces A 83: 273, 1994.
28. B Gestblom, H Førdedal, J Sjøblom. J Dispers Sci Technol 15: 449, 1994.
29. AN Kolmogorov. Dokl Akad Nauk USSR 66: 825, 1949.
30. JO Hinze. AIChE J 1: 289, 1955.
31. PH Clay. Proc Roy Acad Sci (Amsterdam) 43: 852 and 979, 1940.
32. AJ Karabelas. AIChE J 24: 170, 1978.
33. CA Sleicher. Jr. AIChE J 8: 471.
34. HI Paul, CA Sleicher Jr. Chem Eng Sci 20: 57, 1965.
35. SB Collins. PhD thesis, Oregon State University, Corvallis, OR, 1967.
36. FD Rumscheidt, SG Mason. J Colloid Sci 16: 238, 1961.
37. CE Rosenkilde. Proc Roy Soc A312: 473, 1969.
38. CTR Wilson, GI Taylor. Proc Camb Phil Soc 22: 782, 1925.
39. TJ Williams. PhD thesis, University of Southampton, UK, 1989.
40. J Zeleny. Phys Rev 10: 1, 1917.
41. G Taylor. Proc Roy Soc A280: 383, 1964.
42. SK Friedlander, CS Wang. J Colloid Int Sci 22: 126, 1966.
43. PG Saffman, JS Turner. J Fluid Mech 1: 16, 1956.
44. HJ Pearson, IA Valioulis, EJ List. J Fluid Mech 143: 367, 1984.
45. L Prandtl. The Essentials of Fluid Dynamics, Blackie and Son Ltd. 1952.
46. J Nikuradse. Ing Arch 1: 306, 1930.
47. LC Waterman. Chem Eng Progr 61: 51, 1965.
48. W Krasny-Ergen. Ann Phys 27: 459, 1936.

59. TG Oweberg, GC Fernish, TA Gaukler, J Atmos Sci 20: 153, 1963.
50. JA Kitchener, PE Musselwhite. The Theory of Stability in Emulsions. Emulsion Science. New York: Academic Press, 1968.
51. SE Sadek, CD Hendricks. Ind Eng Chem Fundam 13: 139, 1974.
52. RA Mohammed, AI Bailey, PF Luckham, SE Taylor. Colloids Surfaces A 80: 223, 1993.
53. RA Mohammed, AI Bailey, PF Luckham, SE Taylor. Colloids Surfaces A 80: 237, 1993.
54. RA Mohammed, AI Bailey, PF Luckham, SE Taylor. Colloids Surfaces A 83: 261, 1994.
55. SE Taylor. Trans I Chem E 74 (part A): 526 1996.
56. Y Mori, M Tanigaki, N Maehara, W Eguchi. J Chem Eng Jpn 27: 340, 1994.
57. SS Wang, CJ Lee, CC Chan. Sep Sci Technol 29: 159, 1994.
58. T Hano, T Ohtake, K Takagi, J Chem Eng Jpn 21: 345, 1988.
59. K Fujinawa, M Morishite, M Hozawa, N Imaishi, H Ino. J Chem Eng Jpn 17: 632, 1984.
60. PJ Bailes, SKL Larkai. Trans I Chem E 60: 115, 1982.
61. PJ Bailes, SKL Larkai. Chem Eng Res Design 62: 33, 1984.
62. FM Joos, RWL Snaddon. Chem Eng Res Design 63: 305, 1985.
63. PJ Bailes, SKL Larkai. Chem Eng Res Design 65: 445, 1987.
64. PJ. Bailes. Trans I Chem E 73 Part A: 559, 1995.
65. V Gomis. Trans I Chem E 71 (part A): 85 1993.
66. J Drelich, G Bryll, J Kapczynski, J Hupka, JD Miller, FV Hanson. Fuel Process Technol 31: 105, 1992.
67. GW Sams, FL Prestridge, MB Inman. US Patent 5 565 078, 1996.
68. GW Sams, FL Prestridge, MB Inman, KD Manning. US Patent 5 575 896, 1996.
69. US Patent 5 645 451.
70. JP Berry, SJ Mulvey, O Urdahl, AG Bailey, MT Thew, NJ Wayth, TJ Williams. US Patent Application 09/090 060, 1998.
71. O Urdahl, TJ Williams, AG Bailey, MT Thew. Chem Eng Res Design 74 (A2): 158, 1996.
72. O Urdahl, P Berry, NJ Wayth, TJ Williams, KH Nordstad, AG Bailey, MT Thew. Proceedings of the 73rd SPE Annual Technical Conference and Exibition, New Orleans, 1998, SPE Paper 48990, p 111.
73. IG Harpur, NJ Wayth, AG Bailey, MT Thew, TJ Williams, O Urdahl. Electrostatics 40/41: 135, 1997.
74. NJ Wayth, TJ Williams, AG Bailey, MT Thew, O Urdahl. Proceedings of Electrostatics 99 Conference, Cambridge, UK, 1999.
75. I Provost, A Rojey. US Patent 5 643 469, 1997.
76. I Provost, A Rojey. US Patent 5 647 981, 1997.
77. M Smoluchowski. PhysZ 17: 557, 1916.
78. M Smoluchowski. Phys Chem 92: 129, 1917.
79. GR Zeichner, WR Schowalter. AI ChE J 23: 243, 1977.
80. W Findeisen. Meteorol Z 56: 365, 1939.